Experimental and numerical investigation on failure characteristics and mechanism of coal with different water contents

Xuewei Liu[1] · Haixiao Chen[1,2] · Bin Liu[1] · Sai Wang[1,2] · Quansheng Liu[1] · Yong Luo[3] · Jin Luo[2]

Abstract

Water injection, as a widely used technique to prevent coal burst, can restrain the fractured coal seam and released the energy storage. In this study, laboratory tests were firstly carried out on standard coal specimens with five different water contents (i.e., 0%, 0.6%, 1.08%, 1.5%, 2.0%, and 2.3%). The failure mode, fragment size, and energy distribution characteristics of coal specimens were investigated. Experimental results show that strength, elastic strain energy, dissipated energy, brittleness index, as well as impact energy index decrease with increasing water content. Besides, the failure mode transitions gradually from splitting ejection to tensile-shear mixed failure mode as water content increases, and average fragment size shows positively related to water content. Moreover, scanning electron microscope tests results indicate that water in coal sample mainly causes the mineral softening and defects increase. Furthermore, a numerical model containing roadway excavation was established considering the water on coal burst prevention. Modelling results revealed that water injection can reduce degree of coal burst and ejection velocity of coal blocks, while it will raise up the depth of crack zone and surface displacement of roadway. Combined with laboratory tests and numerical results, the micro mechanism, energy mechanism, and engineering significance of water injection on coal burst prevention were finally analyzed.

Keywords Water content · Coal burst · Failure mode · Energy · Numerical simulation

1 Introduction

Coal burst is a common dynamic disaster in coal mine, and it is generally caused by releasing of accumulated energy, which has feature of strong vibration and severe damage to coal and rock mass (Wei et al. 2021; Zhang et al. 2020). In recent years, due to the increase of mining depth, the degree of coal burst intensity and the number of coal burst mines increased significantly (He et al. 2018; Bai et al. 2022). The prevention and control system of coal burst has been initially formed in coal mining, which is mainly divided into two categories: regional prevention and local pressure relief (Mi

et al. 2022; Ma et al. 2022). Regional prevention technology mainly includes reasonable mining of coal seam and control of mining speed (Pan et al. 2022; Zhang et al. 2019); Local pressure relief technology includes borehole pressure relief, coal blasting, coal seam water injection softening (Liu et al. 2018). The construction of regional prevention technology is difficult and cost highly. Therefore, the local pressure relief technology has become the widely used technique for coal burst prevention in engineering.

Water injection, as an important measures of local pressure relief technology, can effectively weaken the mechanical characteristics of coal with help of releasing elastic strain energy stored in coal seam (Li et al. 2022). Water injection is to arrange a number of boreholes and seal them before mining, and then inject pressure water into the borehole to infiltrate into the coal body.

Many scholars analyzed the relationship between water content and the strength of rock or coal to investigate the weakening effect. For rock, tests were conducted on different rock types (such as sandstone (Dou et al. 2020; Zhou et al. 2021; Du et al. 2022), granite (Zhang et al. 2023) and marble (Jiang et al. 2021)) with varying water contents. Results

✉ Bin Liu
   BinLiu5848@163.com

1   State Key Laboratory of Geomechanics and Geotechnical
    Engineering, Institute of Rock and Soil Mechanics, Chinese
    Academy of Sciences, Wuhan 430071, China

2   Faculty of Engineering, China University of Geosciences,
    Wuhan 430074, China

3   Ping'an Mining Engineering Technology Research Institute
    Co., Ltd., Huainan 232001, China

showed that tensile strength, uniaxial compressive strength (UCS), and elastic modulus of rock samples decrease as water content increases. Besides, the relationship between mechanical properties of coal and water content has already been studied. Chang et al. (2021) and Vishal et al. (2015) believed that water content is positively related to peak strain, and it is negatively linear with the compressive strength. Besides, the elastic modulus and water content meet the negative exponentially function. Moreover, some scholars used acoustic emission (AE) technology and scanning electron microscopy (SEM) test to analyze the influence of moisture on the crack propagation of samples. For example, Yao et al. (2019) used to AE, SEM, X-ray diffraction (XRD), and combined with uniaxial compression test. The results showed that AE signal reduces as moisture content increases, because water weakens the connection of coal particles. Gu et al. (2019) found that the strength of soft coal decreases with increasing of water content. Besides, energy theory has been employed to describe the mechanism of this weakening effect (Weng et al. 2019; Liu et al. 2022a, b). The above studies showed that mechanical characteristics of coal (or rock) are closely related to the water content. The mechanical parameters of coal such as UCS, deformation and elastic modulus decrease to varying degrees as moisture content increases, and peak strain increases with increasing of water content. It shows that water has obvious weakening effect on coal and rock.

In summary, a large number of works focused on the influence of water content on the mechanical properties and energy evolution characteristics of coal or rock. However, the mechanism of water softening coal is not clear. Investigations of crack propagation and crack failure mode and the energy evolution characteristics are not abundant. Therefore, it is necessary to clarify the coal softening mechanism in water, explore the effect of water content on energy, and reveal the principles of water injection for coal burst prevention.

In this study, the uniaxial compression tests were first conducted on coal samples with five different water contents to analyze softening law, macroscopic failure mode, and fragment size distribution. Also, the influence of water content on energy and microscopic characteristics were analyzed. Further, based on UDEC numerical simulation, the prevention effect of water injection on coal burst was investigated, and micro and energy mechanism of water on coal burst prevention were finally discussed.

2 Experimental methods and procedures

2.1 Experimental material

Coal samples in this test were collected from Ordos mining area, Inner Mongolia, China. According to XRD test

(Fig. 1). The main minerals of coal are kaolinite and quartz, which accounted for 58.4% and 29.3% of the total mineral components, respectively, and a small number of mineral components are calcite and dolomite, accounting for 9.2% and 3.1%, respectively.

To eliminate the influence of anisotropy and heterogeneity, coal blocks were cut from mining face at same site with similar joints and cracks. The coal block is processed into ϕ50 mm×H100 mm cylindrical samples by wire cutting method in the direction perpendicular to the bedding (Fig. 2a), and the surface of the samples have been polished (Fig. 2b).

To discover the saturated water content of coal, the porosity of coal measured from nuclear magnetic resonance (NMR) tests was compared with the actual result of saturation test. In the saturation test, the coal sample was dried first in an oven at 105 °C for 24 h, and the dried coal sample was weighed. Then, the dried sample put into the vacuum saturated immersed for 24 h. After vacuum saturation, the water on the surface of the sample needs to be cleaned to avoid excessive error, and then weighed. The weight of dried and saturated samples was calculated, and the saturated water content of coal here is 2.94%. Compared with the porosity calculated from NMR test, which is 4.25%, water content pf 2.94% can be identified as the vacuum saturated moisture content of coal.

Furthermore, through the soaking test of coal samples, the relation between water content and soaking time was obtained (Fig. 3). The variation laws of water content with soaking time for of samples are similar. As shown in Fig. 3, the curve contains three stages. The first stage, where the water content of coal increases sharply, is the first eight hours of soaking. The second stage is soaking time from the 8th hour to the 60th hour. At this stage, the growth rate
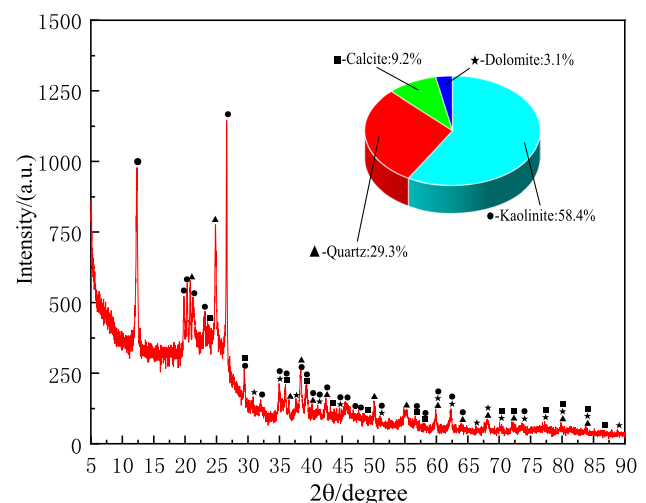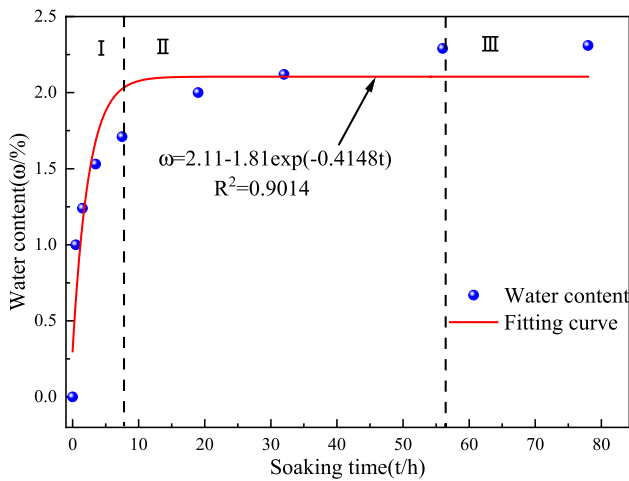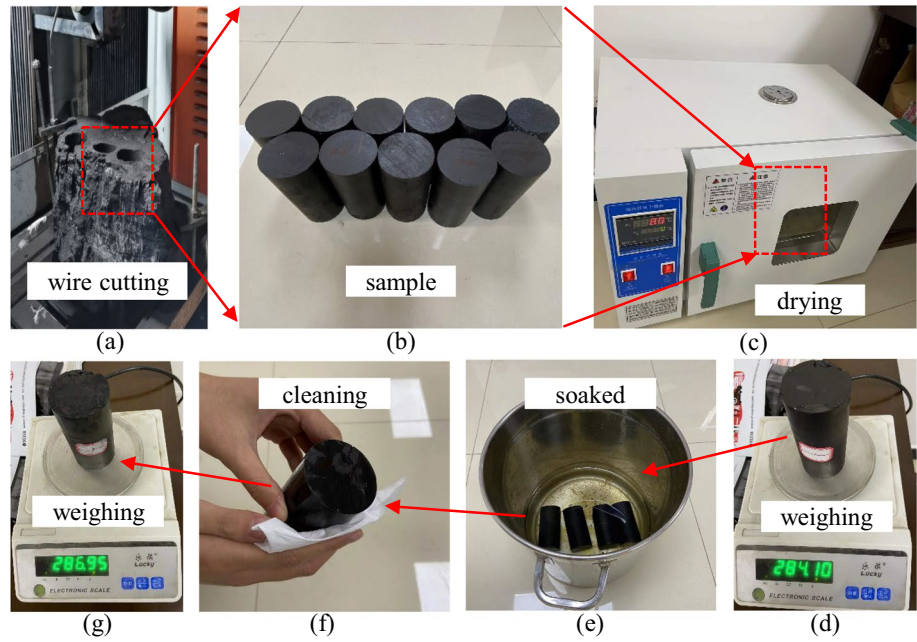

Fig. 1 XRD diffraction curve of coal rock sample

Fig. 2 Preparation processes of coal samples

(a) wire cutting (b) sample (c) drying
(g) weighing (f) cleaning (e) soaked (d) weighing

Fig. 3 Relationship between soaking time and water content

Calculate soaking time according to the set water content and Fig. 3. (2) Put 12 groups of coal samples into drying oven for 24 h, and obtain the weight of the sample, which is recorded as m_0. (3) Soak 12 coal samples with the calculated time from step (1) by natural saturation mode. (4) Weigh the samples after soaked and calculate real water content. The weight of water-soaked sample is recorded as m_i. The water content w_i can be expressed as:

$$w_i = \frac{m_i - m_0}{m_0} \times 100\% \tag{1}$$

2.2 Experimental setup

The tests used the RMT-150C rock mechanics test system, which has four main loading methods (displacement control, load control, stroke control and combination control). The loading rate range of displacement control is 0.0001–1.0 mm/s (13 grades). In this test, displacement control loading was adopted with loading rate of 0.002 mm/s.

The NMR testing equipment is produced by Suzhou Niumai Analysis Instrument Co., LTD. The model is MacroMR12-150H-I, which is mainly composed of magnet, sample holder, data collector and NMR analyzer. The main parameters are: RF pulse frequency is 1–30 MHz, maximum sampling bandwidth is 2000 kHz, magnetic induction intensity is 0.52 T.

of water content began to slow down. The third stage is the 60th hour and later, the water content of this stage is basically keeping constant, it can be considered that the water content reaches saturation with water content of 2.31%.

Five different water contents, including 0% (sample D0), 0.6% (sample D1), 1.08% (sample D2), 1.5% (sample D3), 2.0% (sample D4), and 2.3% (sample D5), were set in tests and two samples were used for each water content. For simplicity, samples D0-1/2 represent the first and second sample with water content of 0%. The preparation process of coal specimens is listed as follows (Figs. 2c–f): (1)

3 Experimental results

3.1 Strength and failure mode

Figure 4 indicates that when the water content increases from 0% to 0.6%, the UCS decreases rapidly from 19.56 to 13.84 MPa, with decrease rate of 9.53, while the decrease rate is 3.34 when the water content increases from 1.08% to 2.30%. A clear transition zone exists within water content range of 0.60%–1.08%. Overall, as water content increases, the UCS showed a nonlinear trend decreasing.
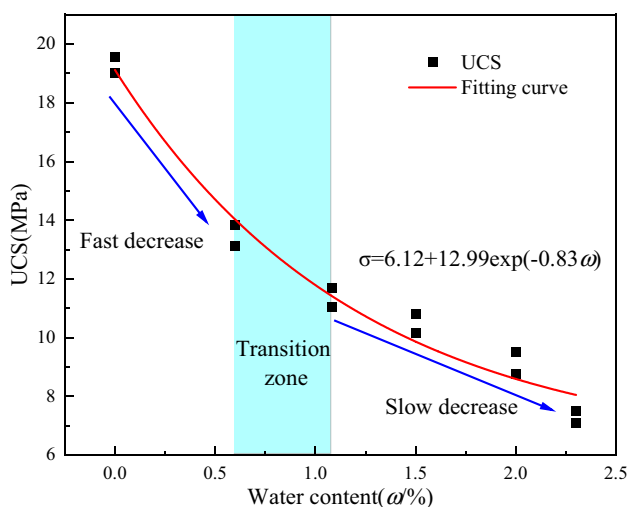

**Fig. 4** Relationship between UCS and water content

The relation between UCS and water content can be fitted as:

$$\sigma = 6.12 + 12.99e^{(-0.83\omega)} \ (R^2 = 0.976) \tag{2}$$

It is obvious from Fig. 5 that the failure characteristics of coal with different water contents are varying. The macroscopic failure modes can be divided into three types: splitting ejection failure mode, tensile shear mixed failure mode and shear failure mode. D0 and D1 occurred splitting ejection failure mode, this mode is severely damaged, and coal sample will break into small pieces and collapse outwards along the splitting band, accompanied by huge sound (Figs. 5a, b) at peak point. Samples D2 and D3 occurred the tensile-shear mixed failure mode. The damage intensity decreases and the collapse is less, but there are more surface spalling areas, and there are more macroscopic tensile cracks and a small amount of macroscopic shear cracks on surface of samples and within the spalling area. Samples D4 and D5 occurred shear failure mode. This failure mode is mainly characterized by the surface falling off from small-scale coal blocks, and more shear cracks occurred. After the shear cracks are interconnected, obvious shear bands are formed, and finally shear failure occurs.

Overall, the water content has a significant effect on failure mode of coal sample. When samples varying from D0 to D5, the failure severity gradually decreases, and the scale of the coal block on the surface gradually decreases.

Fig. 5 Failure characteristics of coal samples with different water contents: **a**, **g** Water content of 0%; **b**, **h** Water content of 0.6%; **c, i** Water content of 1.08%; **d, j** Water content of 1.5%; **e, k** Water content of 2%; **f, m** Water content of 2.3%
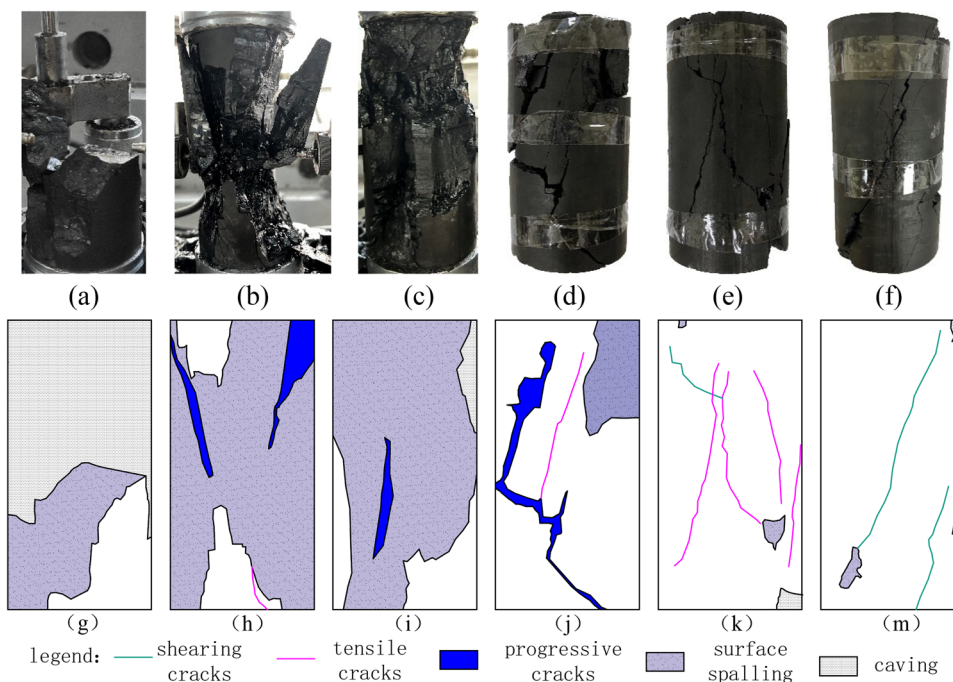
At the same time, the failure mode gradually transitions from splitting ejection to tensile shear mixed, and finally to shear failure mode.

Besides, the failure states for different samples are analyzed. It can be seen from Fig. 6 that the crushing degree decreases as water content increases. For samples D0, it contains dozens of broken coal blocks, the size is relatively small. With the increasing water content from 0.6% to 1.08%, the number of fragment decreases, while the size increases. When the water content increased to 1.5%, the broken coal samples began to appear larger coal blocks, and the broken samples contain both of larger coal blocks and some smaller fragments. For samples D4 and D5, the coal sample presents a standard shear failure mode, and the whole coal sample is relatively intact, only a small number of fragments were observed.

3.2 Fragment size distribution

To analyze the fragment size distribution characteristics, the blocks of failure coal were collected carefully after each test. Then, the collected coal was taken back to the laboratory for screening with a standard sieve (Fig. 7). The standard screen diameters used in this test includes 10 grades (from 1.2 to 40 mm).

Figures 8 and 9 displayed typical broken fragment size distribution of failure coal samples D0 and D5. It is clearly that when the water content is 2.3%, most of the coal samples were broken with particle size greater than 40 mm and particle size between 40 and 31.5 mm. When the water content is 0%, the broken particle size greater than 40 mm and particle size between 40 and 31.5 mm was significantly smaller than samples D5, and the broken particles are mainly concentrated in the particle size between 25 and 1.2 mm.
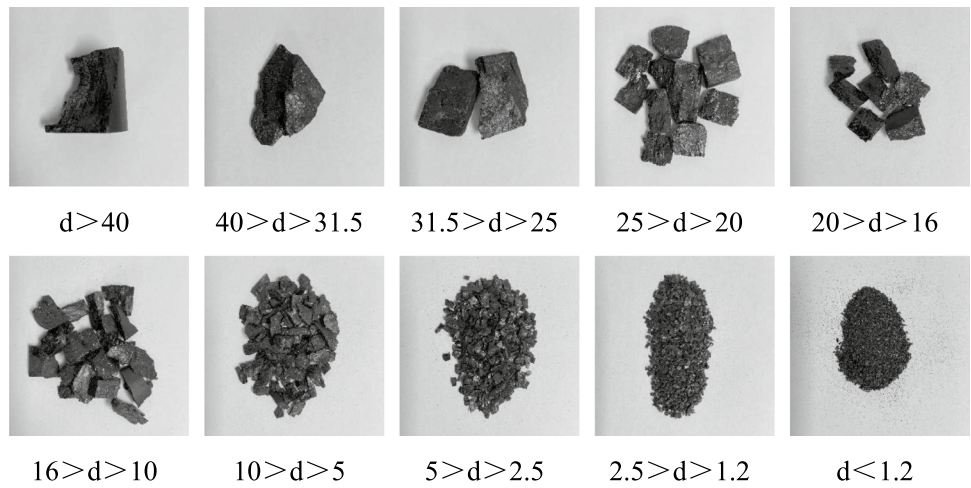
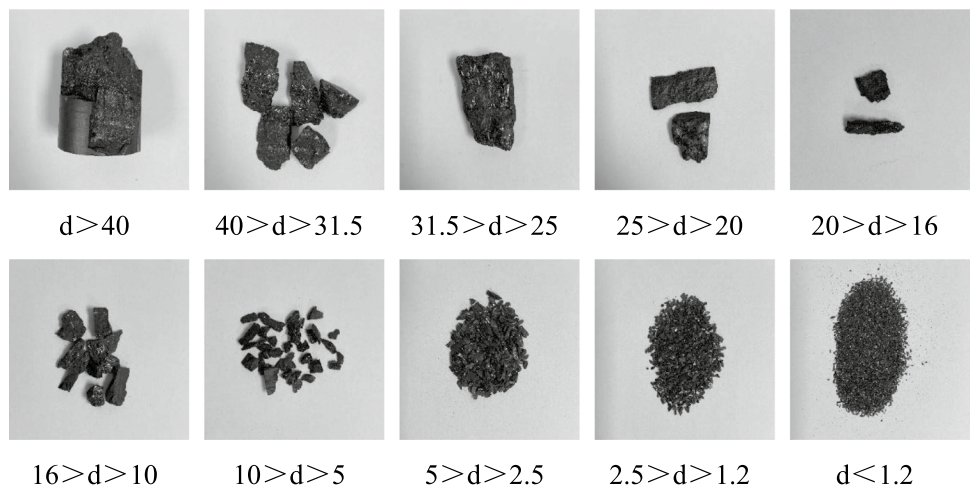**Fig. 6** Failure states of coal specimens under different water contents
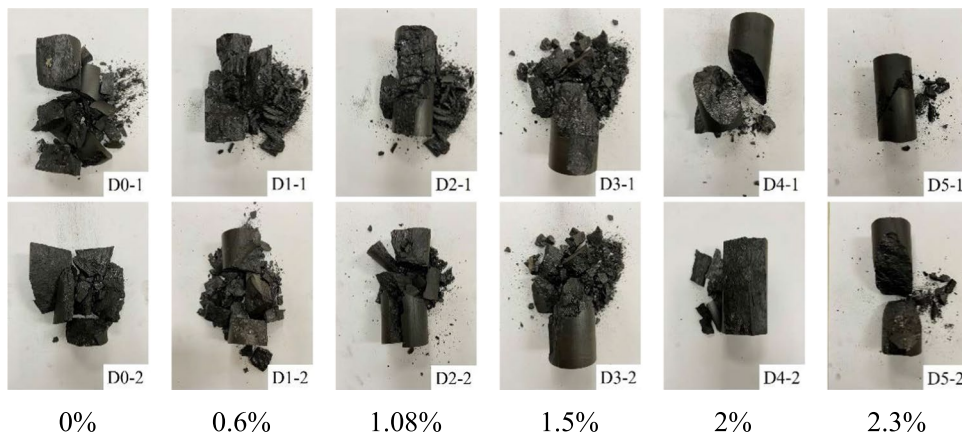
Fig. 7 Standard sieve for screening broken coal samples

Fig. 8 Distribution of particle size with 0% water content. (Unit: mm)

| d>40 | 40>d>31.5 | 31.5>d>25 | 25>d>20 | 20>d>16 |

| 16>d>10 | 10>d>5 | 5>d>2.5 | 2.5>d>1.2 | d<1.2 |

Fig. 9 Distribution of particle size with 2.3% water content. (Unit: mm)

| d>40 | 40>d>31.5 | 31.5>d>25 | 25>d>20 | 20>d>16 |

| 16>d>10 | 10>d>5 | 5>d>2.5 | 2.5>d>1.2 | d<1.2 |

Specifically, Fig. 10a showed that cumulative weight percentage of coal fragments under different water contents. Generally, the slope of the curve can reflect the percentage of coal fragments in a certain diameter interval. When the water contents are 0% and 0.6%, the maximum slope appears in range of 20 mm–25 mm, with weight percentage of 26.2% and 23.2%. For sample with water content of 1.08%, the maximum slope is in range of 25–31.5 mm, accounting for 26.2% of the whole sample weight. For samples D3, D4, and D5, the maximum slope is fragment size over 40 mm, with weight percentage of 42%, 61%, and 63.1%, respectively. It is clearly that the size of the maximum percentage interval of coal particles increases as water content increases.

Furthermore, the parameters of average fragment size can be defined as (Weng et al. 2019):

$$d_m = \frac{\sum (w_i d_i)}{\sum w_i} \tag{3}$$

where d_i and w_i are the average size between two screens and the percentage of the weight of fragments between the corresponding two screens, respectively.

The influence of water on average fragment size was further investigated. From Fig. 10b, it is evident that the average fragment size of failure coal sample increases from 24.16 to 38.36 mm as water content increases from 0% to 2.3%. Compared Fig. 4 with Fig. 10b, it is noticeable that the fragment size distribution of coal samples is negatively correlated with its UCS. Therefore, as water content increases, the UCS decreases, and failure mode gradual change, the number of fragments decrease, while the average fragment size increases.

3.3 Coal energy distribution

Figure 11 shows the definition of energy parameter. The work done by external force is the total energy U_p (area o-a-b-c-h in Fig. 11). Part of the strain energy is exchanged to releasable elastic strain energy U_p^e (e-c-h) stored, the other part is dissi-
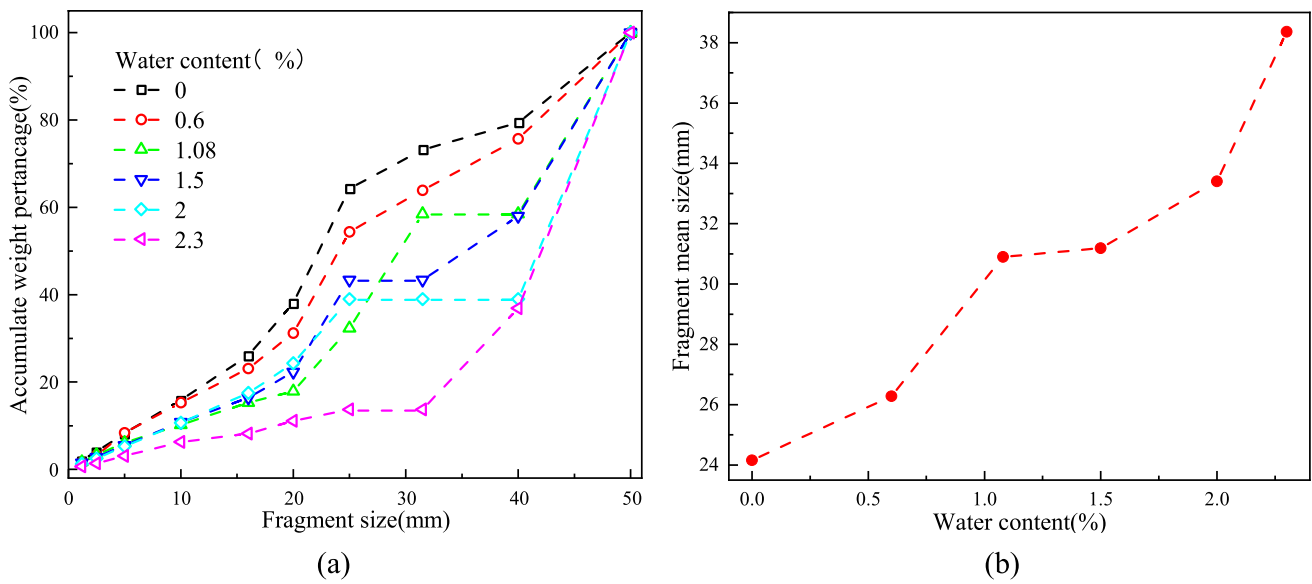
Fig. 10 Fragment size distribution characteristics: **a** Cumulative percentage of coal fragments; **b** Relationship between fragment average size and water content
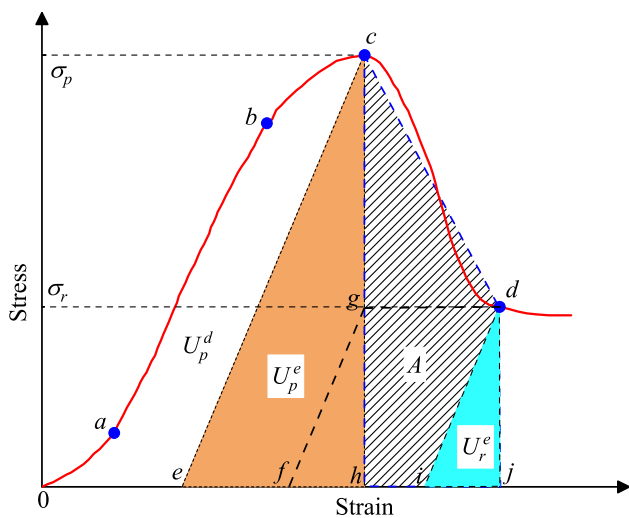
Fig. 11 Energy parameters definition

pated in form of dissipated energy (DE) U_p^d (o-a-b-c-e), which can be expressed as:

$$U_p = U_p^e + U_p^d \tag{4}$$

The total energy (TE) absorbed by coal samples under uniaxial compression can be calculated by:

$$U_p = \int \sigma_1 d\varepsilon_1 = \sum_{i=0}^{n} \frac{1}{2}(\varepsilon_{1i+1} - \varepsilon_{1i})(\sigma_{1i+1} + \sigma_{1i}) \tag{5}$$

The elastic strain energy (ESE) can be obtained by following:

$$U_p^e = \frac{1}{2}\sigma_1\varepsilon_1^e \tag{6}$$

According to Hooke's law:

$$U_p^e = \frac{1}{2}\sigma_1\varepsilon_1^e \approx \frac{\sigma_1^2}{2E_0} \tag{7}$$

here, σ_1 and ε_1 are uniaxial stress and strain. Parameters σ_i and ε_i are stress and strain at each point at the stress–strain curve, which are determined from the recorded data during test. Parameter n and i are number and corresponding data in the stress strain curve. E_0 is initial elastic modulus. ε_1^e is the elastic strain value.

The residual strain energy (RSE) at post peak can be calculated by the following:

$$U_r^e = \frac{\sigma_r^2}{2E_0} \tag{8}$$

where U_r^e is residual strain energy, σ_r is residual stress.

The energy parameters for different samples were calculated by the above equations. Figure 12a showed relationship between the average values of the calculated energy and water contents. It can be obviously seen that the TE, ESE as well as DE decrease significantly with increasing of water content. Among them, the TE and ESE decrease fast as water content increase, while the DE has a tiny decrease from 13.09 to 4.38 kJ/m³, approximately 67%.
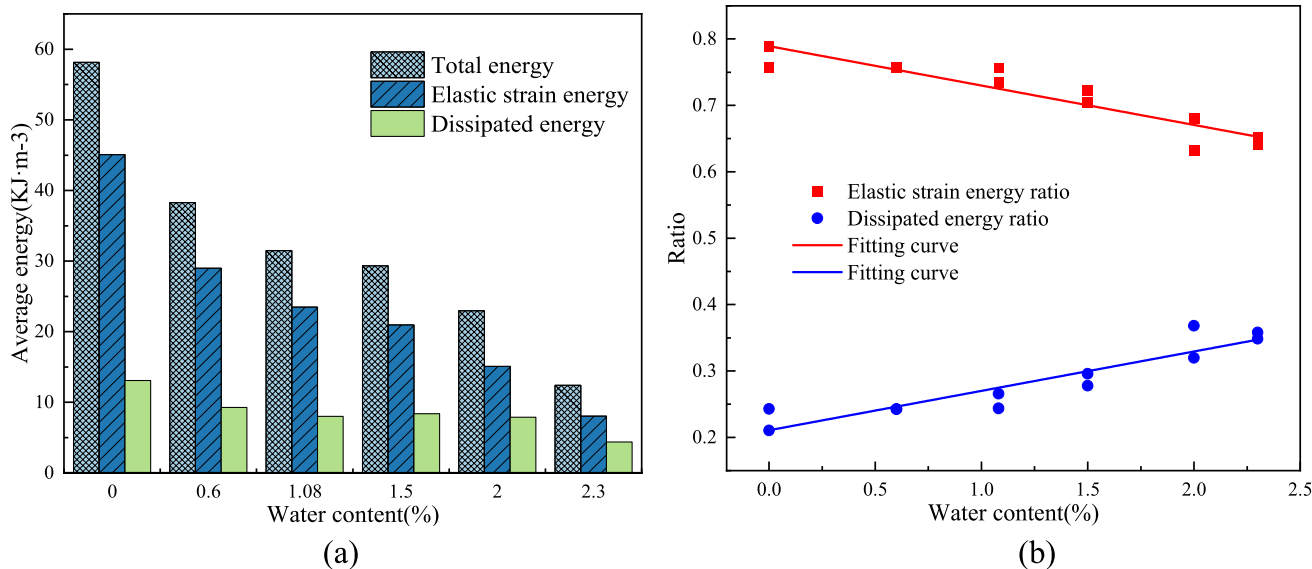
Fig. 12 Energy diagram of coal samples with different water content: **a** Energy parameters; **b** E_r and D_r

Two parameters, namely elastic strain energy ratio (E_r) and dissipated energy ratio (D_r), were proposed here to investigate energy laws. The elastic strain energy ratio is defined as the ratio of ESE to TE, which is:

$$E_r = \frac{U_p^e}{U_p} \tag{9}$$

The dissipated energy ratio (D_r) is defined as the ratio of DE to TE, which is shown as follows:

$$D_r = \frac{U_p^d}{U_p} \tag{10}$$

Relationship between E_r, D_r, and water content are obtained by linear fitting. From Fig. 12b, it is evident that the Er decreases while D_r increases linearly as the water content increases.

Generally, the occurrence of coal burst is coupled with the accumulation and release of energy. The factor of IEI (K_E) is regarded as a criterion parameter in the rock burst proneness (Zhang et al. 2022), which is the ratio of ESE to fracture released energy, and can be obtained as following:

$$K_E = \frac{U_p^e}{A} \tag{11}$$

where A is fracture released energy.

Here, the relationship between the impact energy index and water content (Fig. 13) indicated that the IEI of coal samples shows a negatively correlated with water content. When the water content is 0%, the average IEI is 4.85,
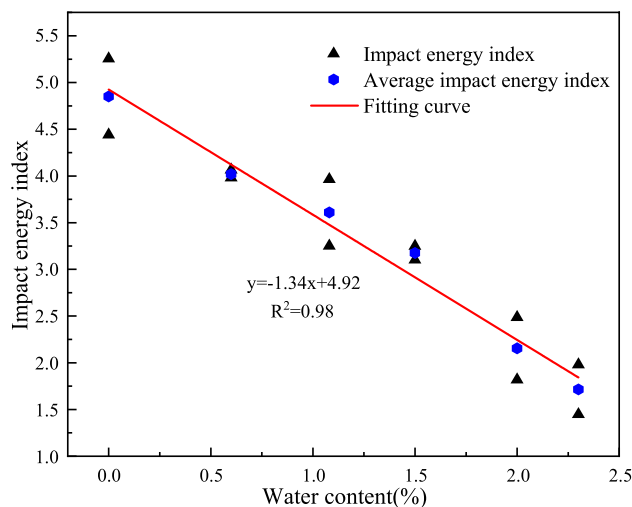

Fig. 13 Relationship between impact energy index and water content

and this value decreased to 1.72 when the water content increases to 2.3%.

In summary, with increasing water content, the elastic strain energy ratio (E_r) decreases, while the dissipated energy ratio (D_r) increases. Therefore, the water in coal causes increase in proportion of dissipated energy, and finally results in decreasing of impact energy index and burst proneness.

3.4 Microscopic characteristics

The influence of different water content on the microstructure of coal samples was investigated by SEM tests.

Figure 14 shows the microscopic SEM images of coal samples with amplified 5000 times under different water content. It is obvious that as water content increases, The kaolinite gradually transforms from dense to loosen structure, while quartz changes much. The mineral particles from the surface smooth, dense structure gradually transformed into a loose surface, flocculent structure, which can be called softening zone. With increasing water content, the softening zone, cracks, and porosity of coal samples increase, while the number of pores decreases. For samples D0, it is compact structure and contains some pores. For sample D1 (water content of 0.6%), the softening zone begin to appear (yellow area in the Fig. 14b), and the mineral particles in the softening zone become obviously rounder and smoother than that of D0. As same time, the pores between mineral particles are enlarged. When the water content increase to 1.5%, the softening zone is more obvious, and the corners between mineral particles are gradually smooth, and the surface begins to show signs of loosening. When the water content increase to 2.3%, the surface appeared many loose clusters and flocculent structures. The whole coal sample is almost covered by softening zone, and the particles in the sample are loose. Therefore, the internal water content can change the microstructure and soften part of minerals of coal sample, which finally influences the mechanical properties.

4 Numerical simulations

4.1 Numerical model configuration

To study the effect of water on deformation and failure of roadway during excavation, numerical simulations were carried out by Universal Distinct Element Code (UDEC). In UDEC Voronoi model, Voronoi blocks can move and rotate once the contacts between them satisfied the given constitutive rules. Therefore, this model can also simulate cracking, movement, and rotation of blocks effectively. Besides, UDEC flow code can also simulate the fluid flowing process in fracture networks. Therefore, UDEC Voronoi model is very suitable for investigating coal burst process under different conditions here.

22103 working face of Yingpanhao Coal mine in Ordos mining area has a thick coal seam (4.6 m, approximately). According to Strata histogram (Fig. 15), the numerical model has been established with 50 m in width and 47.5 m in height. This model contains three parts, namely roof (fine sandstone, mudstone and sandy mudstone, 24.9 m in thickness), coal seam (4.6 m in thickness), and floor (mudstone, sandy mudstone, and siltstone, 18 m in thickness). Specially, the width of coal roadway is 3 m, and a further
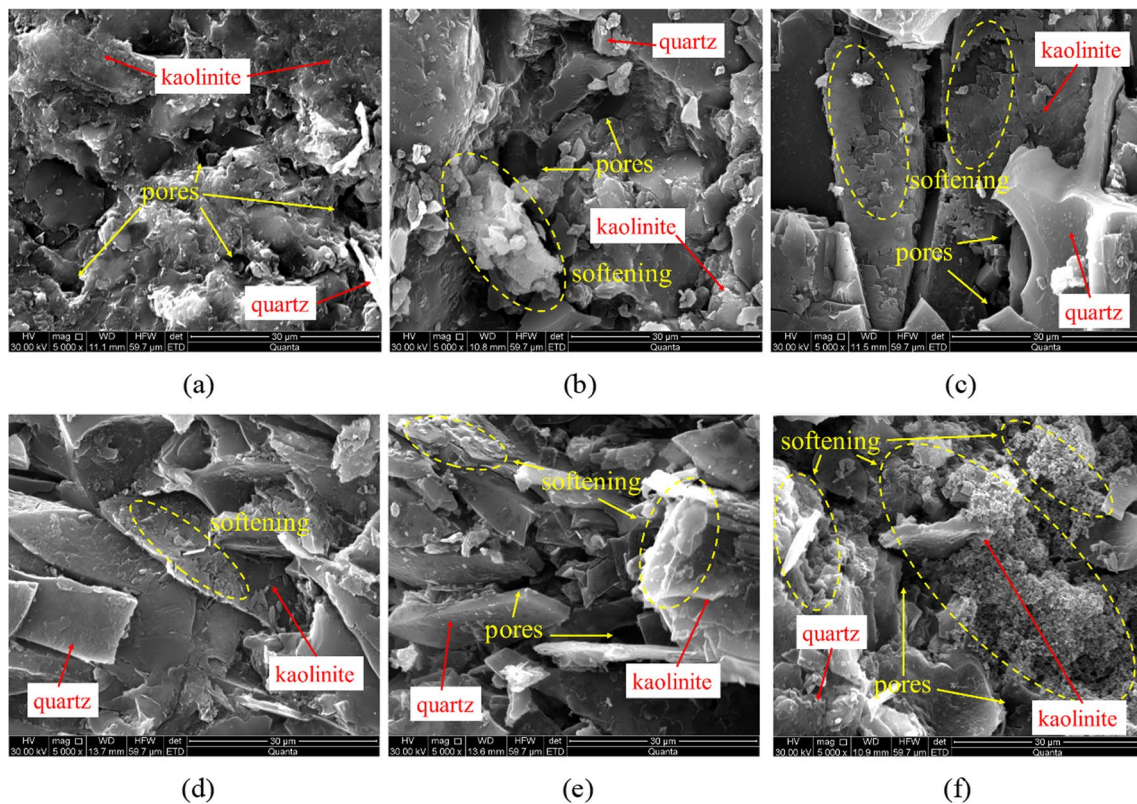

Fig. 14 SEM results for different water contents: **a** 0%; **b** 0.6%; **c** 1.08%; **d** 1.5%; **e** 2%; **f** 2.3%
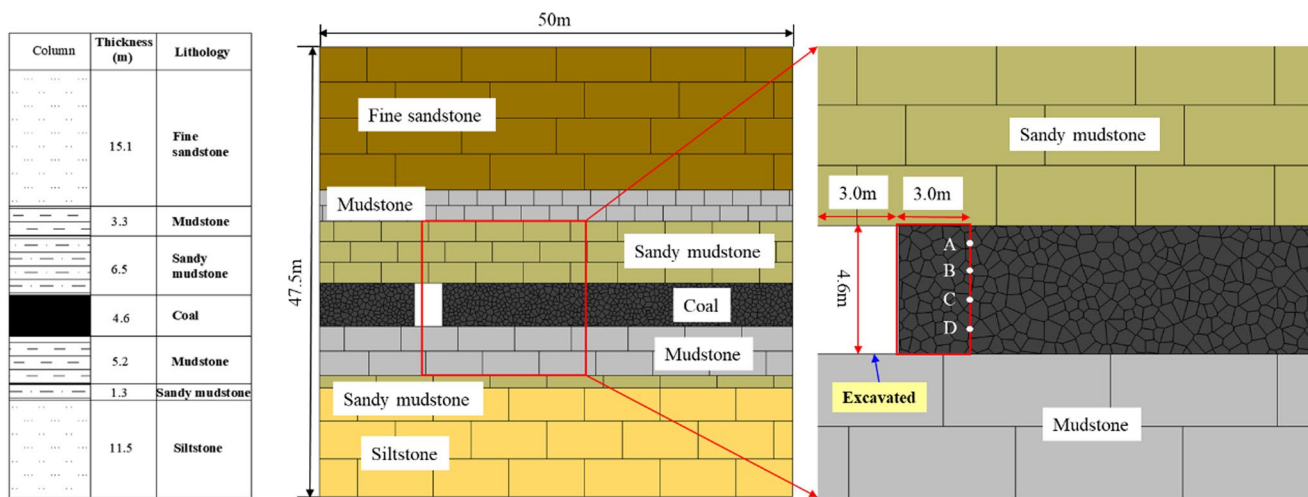
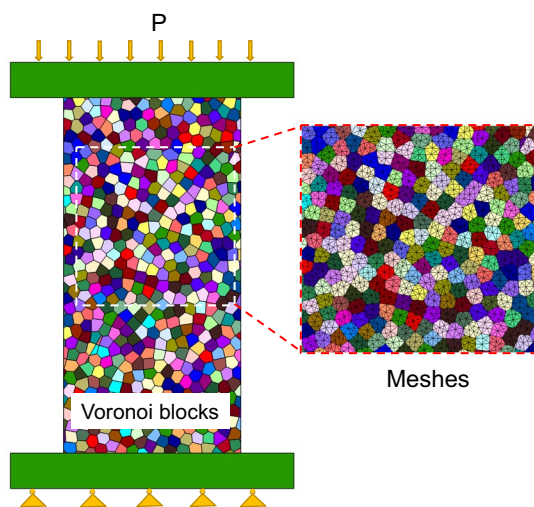**Fig. 15** Numerical simulation model for No. 22103 working face

Fig. 16 UDEC parameter calibration uniaxial compression calculation model

3 m coal seam will be excavated along advance direction during numerical calculation. In this model, the coal seam is divided into random Voronoi blocks with average length of 0.4 m. Four monitoring points, with coordinates of A ($x = 16.0$ m, $y = 21.68$ m), B ($x = 16.0$ m, $y = 20.76$ m), C ($x = 16.0$ m, $y = 19.84$ m), and D ($x = 16.0$ m, $y = 18.92$ m), are set to monitor the deformation and block velocity of coal seam surface in x-direction.

As shown in Fig. 16, a UDEC uniaxial compression model parameters of the coal sample under dried and saturated conditions were calibrated by the trial-and-error method (Shen

et al. 2020). In this model, the coal sample is random Voronoi block, with deformable mesh in it. As shown in Figs. 17a and d, for dry and saturated specimens, the error percentages of uniaxial compressive strength between numerical and laboratory tests are 2.9% and 4.3%, respectively. For the failure of samples, as shown in Figs. 17b and e, it can be found that under dry conditions, the sample has obvious coal block ejection and spalling failure mode, while the saturated sample has a gradually penetrating fracture zone and a local tensile failure occurred in dry sample, which are consistent with the test results (Figs. 18c and f). Through the above research, the parameters of UDEC model are finally determined and shown in Table 1.

4.2 Numerical results

As shown in Fig. 15, two cases are used to evaluate the coal burst prevention of water injection. In case 1, the coal seam is dry state. After the initial stress balance, the coal seam will be excavated three meters (red rectangular in Fig. 15). In Cases 2, the water injection first applied and then excavating. After the initial stress is balanced, the water is fully injected through the water injection hole. Five water injection holes, with coordinates of W1 ($x = 19.0$ m, $y = 20.3$ m), W1 ($x = 22.0$ m, $y = 20.3$ m), W1 ($x = 25.0$ m, $y = 20.3$ m), W4 ($x = 28.0$ m, $y = 20.3$ m), and W5 ($x = 31.0$ m, $y = 20.3$ m), are set in the coal seam area. The water injection pressure is set as 1.0 MPa. For simplicity, the coal seam with fracture water pressure greater than 1.0 kPa is assumed as saturated state, while otherwise is dry state.
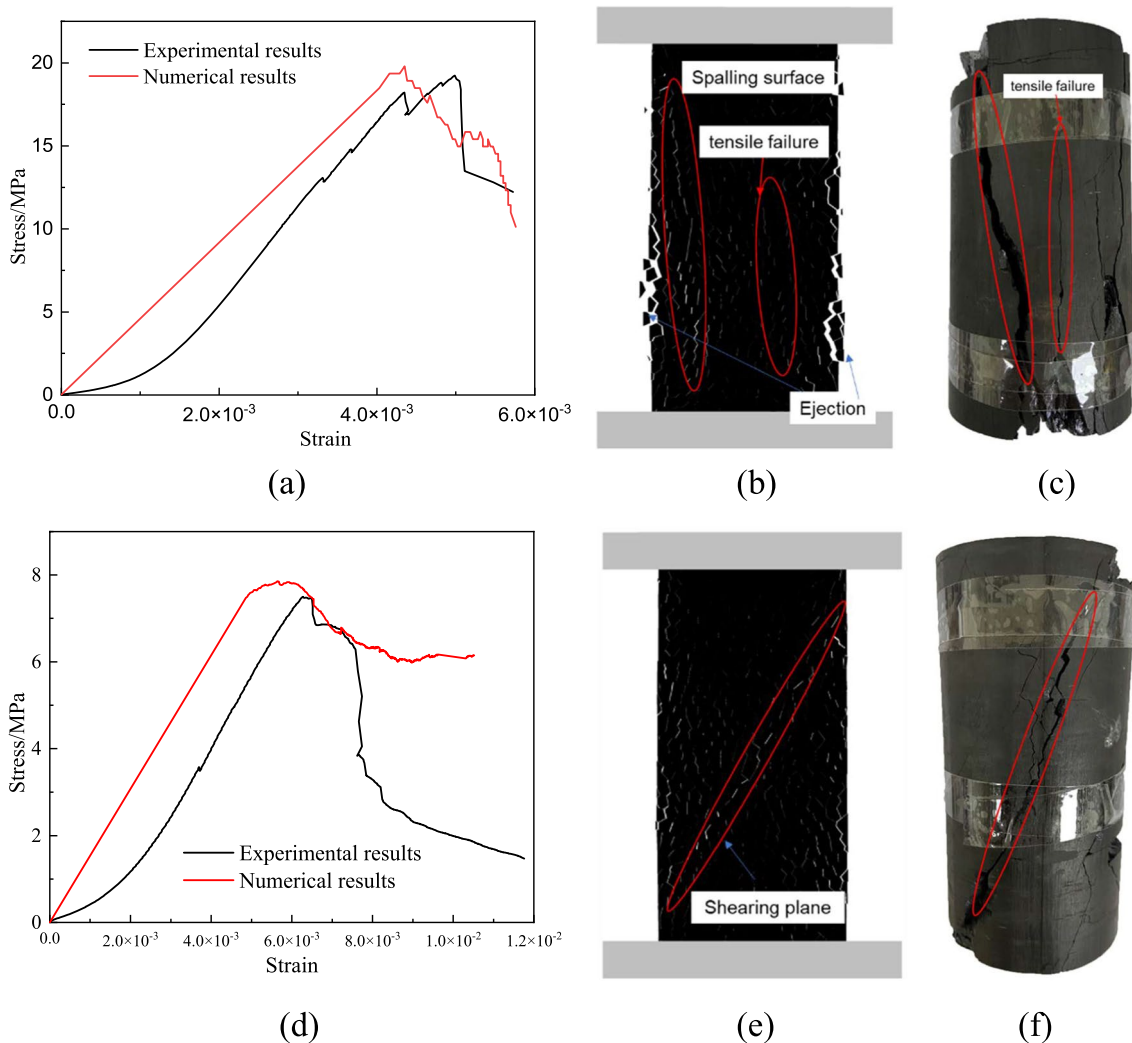
Fig. 17 Parameter calibration of dry and saturated samples: **a**, **b**, **c** Stress strain curve, numerical and experimental final failure mode of dry sample; **d**, **e**, **f** Stress strain curve, numerical and experimental final failure mode of saturated sample
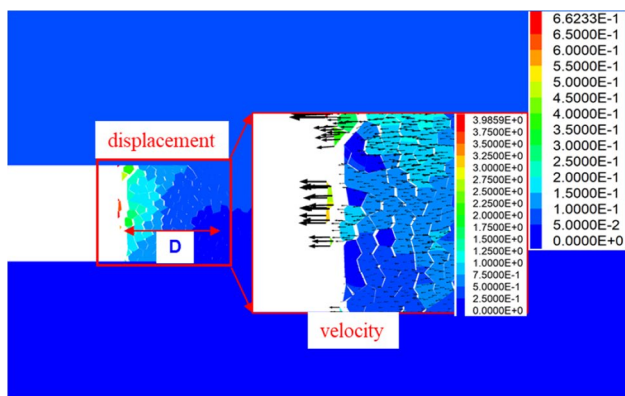
(1) Case 1

Figure 18 displayed displacement distribution and final failure mode of case 1. Overall, the final displacement distribution shows a vertical distribution, which indicates that the surrounding rock has the same displacement in a certain depth range of the roadway surface. According to the monitoring results, the maximum velocities for the top and middle blocks are 3.98 and 3.06 m/s, respectively. Therefore, an obvious layered spalling failure characteristics is occurred here. As shown in Fig. 18b, there are two obvious coal blocks ejection, especially the coal block in the middle of the roadway has flown 0.52 m away from the surface of the roadway approximately. The failure of coal seam also shows different characteristics in the process

from the surface to the inside. The surface of the roadway is splitting failure. With the increase of depth, the failure mode is crack propagation. The crack apertures for these newly generated cracks gradually decrease until no coal seam failure occurs as the depth increases. At this time, the final depth is defined as depth of crack zone (D). In case 1, the depth of crack zone (D) reached up to 4.51 m at the end of simulation.

(2) Case 2

Figure 19 shows the displacement distribution and failure mode of case 2. The displacement forms a V shaped concentration area on the roadway surface, which is characterized by slip failure of sidewall of roadway. As the depth
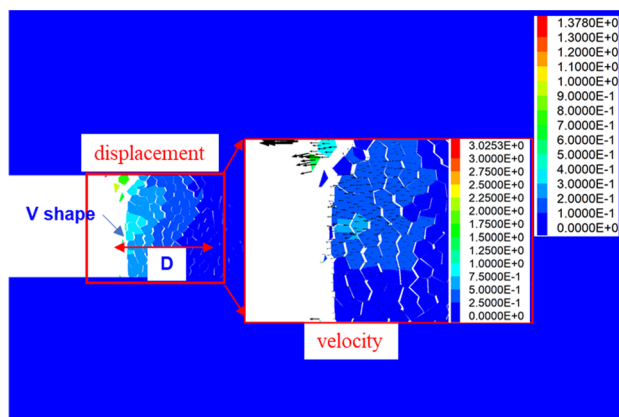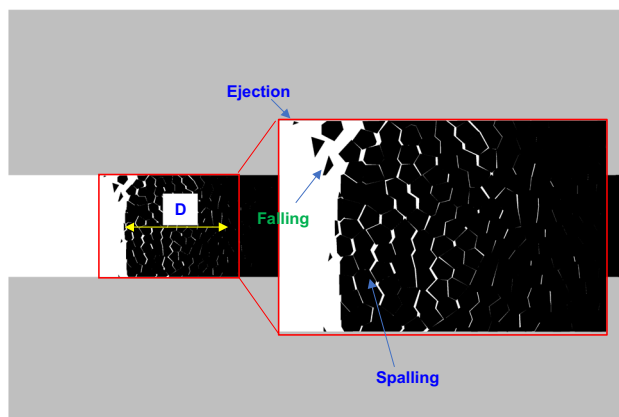
(a)
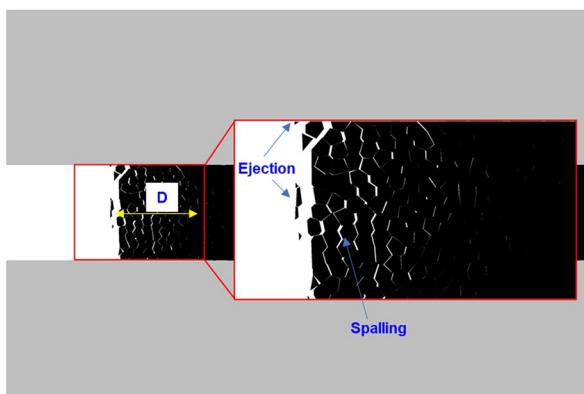
(b)

Fig. 18 Numerical simulation results of case 1 **a** Final displacement distribution **b** Final failure mode

(a)

(b)

Fig. 19 Numerical simulation results of case 2 **a** Final displacement distribution **b** Final failure mode

increases, the displacement distribution gradually converts to the vertical distribution, which is spalling failure. According to the monitoring results, the ejection falling speed of the top coal blocks and are 3.02 and 1.57 m/s, respectively. The speed of all the other blocks is less than 0.5 m/s. As shown in Fig. 19b, there is a small coal block ejection and some blocks fall at the top of roadway. However, the middle and bottom of surface are basically stable. There is an obvious interlayer spalling failure mode in surrounding rock, and the depth of crack zone is 5.93 m, approximately.

4.3 Analysis of numerical results

Figure 20 showed the final crack patterns in coal seam under different cases. The red and green lines indicate tensile and shear cracks, respectively. After excavation of coal, the distribution of crack types is nearly same for these two cases. The tensile cracks formed on surface and most visible failure zone of roadway in surrounding rocks.

Table 1 Parameters of UDEC model

Lithology	Intact rock			Joints				
	ρ (kg/m^3)	K (GPa)	G (GPa)	k_n (GPa/m)	k_s GPa/m	c_j (MPa)	φ_j (°)	σ_{ij}(MPa)
Fine sandstone	2600	4250	10,525	125	62	8.4	32	7.1
Siltstone	2600	4130	10,324	122	58	7.6	25	6.4
Sandy mudstone	2410	3436	9249	114	54	7.1	22	6.2
Mudstone	2350	3274	9126	101	48	6.3	19	5.7
Coal (drying)	1410	591	232	11.24	6.31	0.84	16	0.21
Coal (saturated)	1435	307	154	10.33	5.24	0.23	9	0.06

While most of shear cracks only occurred at the deeper area, where there are no evident cracks opening. Besides, both the amount and coverage area of shear and tensile cracks of case 2 are larger than that of case 1, which is closely related to water injection in coal seam. In case 2, water injection causes high water pressure in cracks of coal seam, and the cracks may open or even failure under the water pressure. Therefore, the coal seam with water injection is under condition of coupled hydro-mechanical process and a damage in coal has been occurred in advance, which cause a larger crack zone in coal seam finally.

Figure 21 displayed the displacement distribution of monitoring points during calculation under different cases. For case 1, the displacements for points A and D (top and bottom of roadway) are about 0.15 m, while the largest

displacement occurred at point B with value of 0.63 m and caused by block ejection here. For the case 2, the displacements for points B, C, and D are close to each other. The final displacement for these three points is around 0.3 m. While the final displacement of point A, located at top side of roadway, is about 0.61 m, which caused by the block falling at this place.

Furthermore, Fig. 22 showed the block velocity of monitoring points in coal seam. Overall, for points B and C, the block velocity for case 1 is much larger than that of case 2. Specifically, the maximum velocity of point B for case 1 is 4.71 m/s, and this value decreases to 3.77 m/s in case 2 (Fig. 22c). Similarly, the maximum velocity of point C decreases from 4.46 to 4.34 m/s. It is also clear from Fig. 22c that for both of the maximum and final block
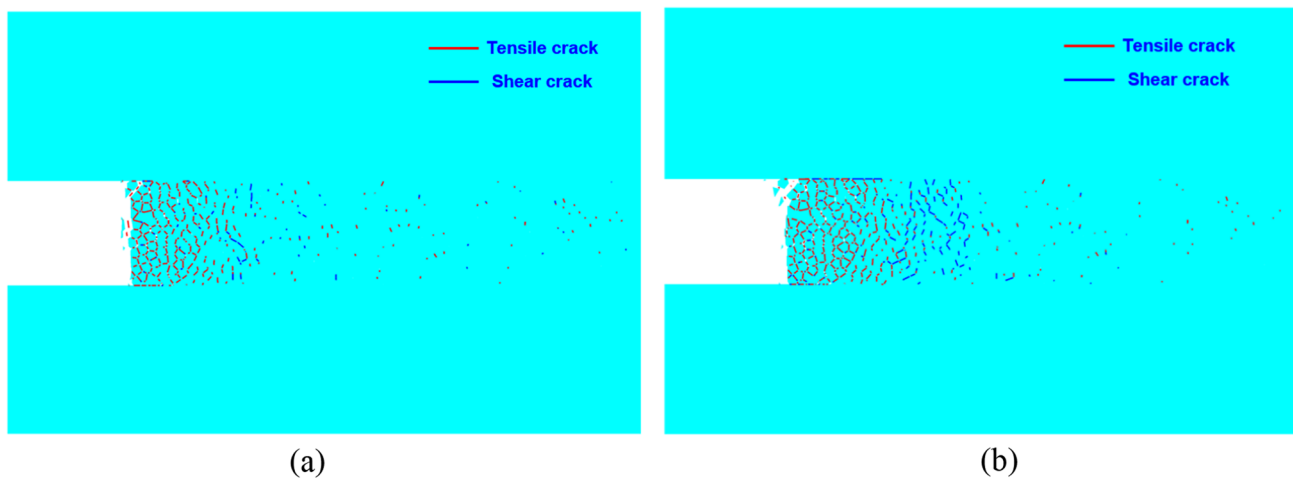

(a)   (b)

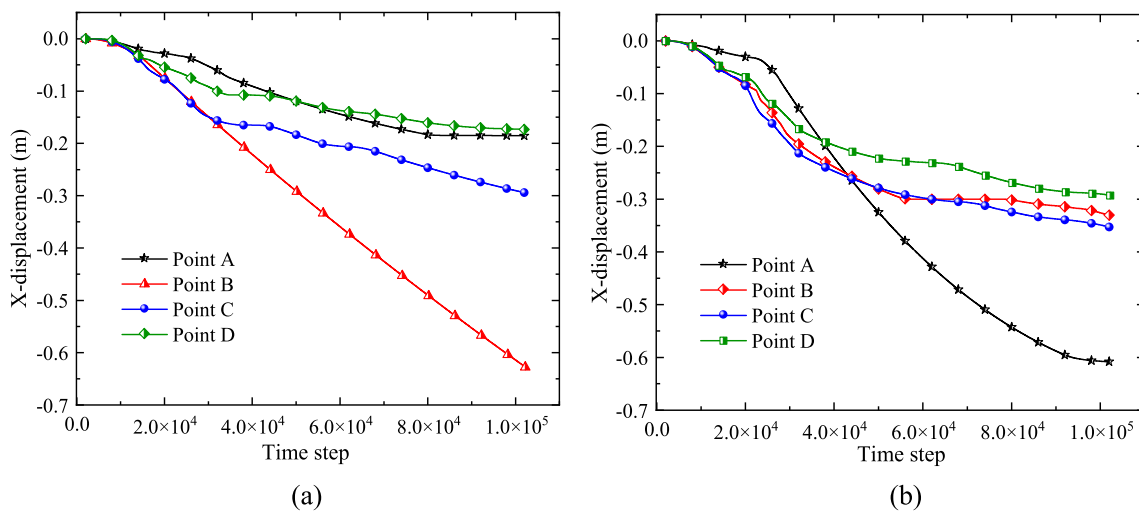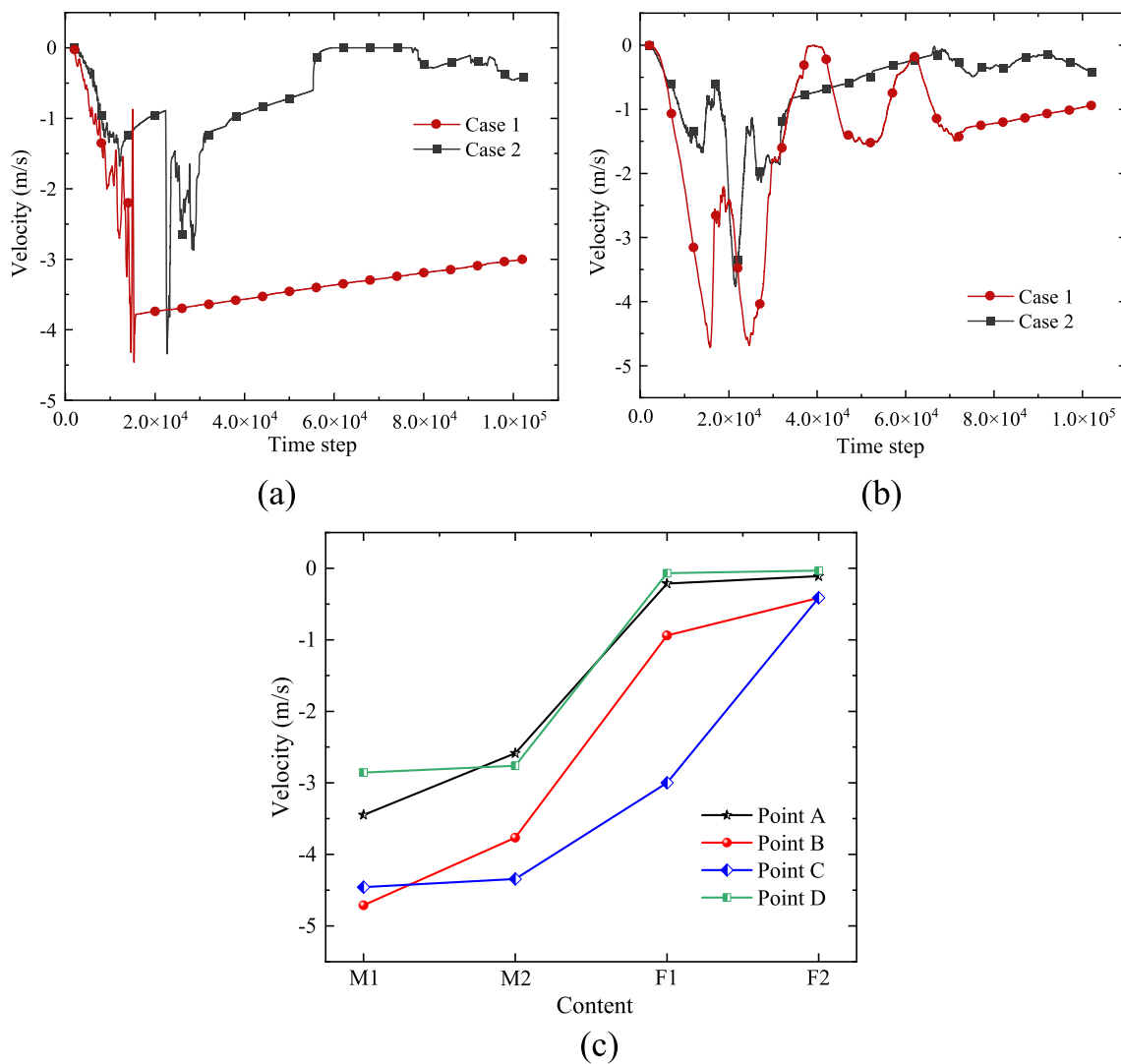**Fig. 20** Cracks in coal for different cases: **a** Case 1; **b** Case 2

(a)   (b)

Fig. 21 Displacement distribution of monitoring points for different cases: **a** Case 1; **b** Case 2

(a)

(b)

(c)

Fig. 22 Block velocity of monitoring points in coal seam: **a** Point B; **b** Point C; **c** Relationship between velocity and different cases. *Note*: M1 and M2 are maximum velocities of case 1 and case2 during cal-culation, respectively. F1 and F2 are final velocities of case 1 and case2 at end of calculation, respectively

velocity, the values of case 1 are always larger than that of case 2 for all points.

From Fig. 12, with increasing of water content, the ratio of ESE decreases while Dr increases gradually. Therefore, the dry coal seam has character of larger ESE and smaller dissipated energy, which may cause more energy can be transferred into kinetic energy. As a result, the broken coal blocks own a larger velocity. To the contrary, for the saturated coal seam, there is a smaller ratio of elastic energy and more energy has been dissipated, which caused a smaller velocity for coal blocks.

5 Discussion

5.1 Micro mechanism of water on coal burst prevention

Figure 23 is micro mechanism according to SEM results. Different colors represent different mineral particles in the diagram. It can be seen that many primary pores existed between minerals inside the coal. There is no free water in these pores for dry coal sample. When coal encounter water, water will enter these pores. the water in the pores gradually

increases as water content increases. When the pores are fully filled with water, the coal sample reaches saturation.

The softening effect of water on coal seam is mainly divided into two parts. (1) The minerals of coal are mainly Kaolinite, Quartz, Calcite and Dolomite. The Kaolinite is clay mineral, which has the property of water absorption and expansion (Wang et al. 2023; Li et al. 2023). Therefore, after water injection, the Kaolinite particles gradually transitions from dense to flocculent structure, which decreases the cementation ability between particles. As a result, the mineral particles fall off and the pores become larger. Si et al. (2021) obtained that clay minerals swell out of the matrix when exposed to water, which increases the number of internal pores in coal sample and reduces the strength. Therefore, as water content increases, the cohesion and internal friction angle between adjacent mineral particles decrease, which is macroscopically characterized by the decrease of coal seam strength. (2) When the saturated coal seam is under loading, the free water existed in pores between particles will flow. At this time, the pore water pressure will increase, resulting in the decreasing of effective stress and rotation of the stress direction around the pores. Han et al. (2023) indicated that the stress state around the pores may transfers from compressive to tensile. Besides, the decreasing of effective stress may also cause decreasing of tensile strength. Therefore, tensile cracking occurs when stress over the tensile strength. When a large number of macroscopic cracks appeared, the coal seam failure.

Figure 24 displayed the above two influence factors of water content by the Mohr circle strength envelope. Compared with the diagram of water injection softening mechanism in Fig. 26, the expansion of clay minerals in coal seam with water will lead to the decrease of the cohesion and internal friction angle of coal seam, which moves down and reduce the slope of the strength envelope. Besides, with existence of effective stress, the Mohr circle moves to the left with distance of pore water pressure. Because the two parts weakening mechanism listed above, the Mohr circle moves to the left and the strength envelope moves downward, which makes saturated coal sample failure easier. The result here is consistent with Hao et al. (2020).
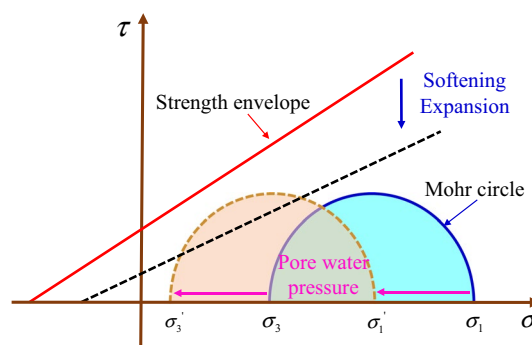

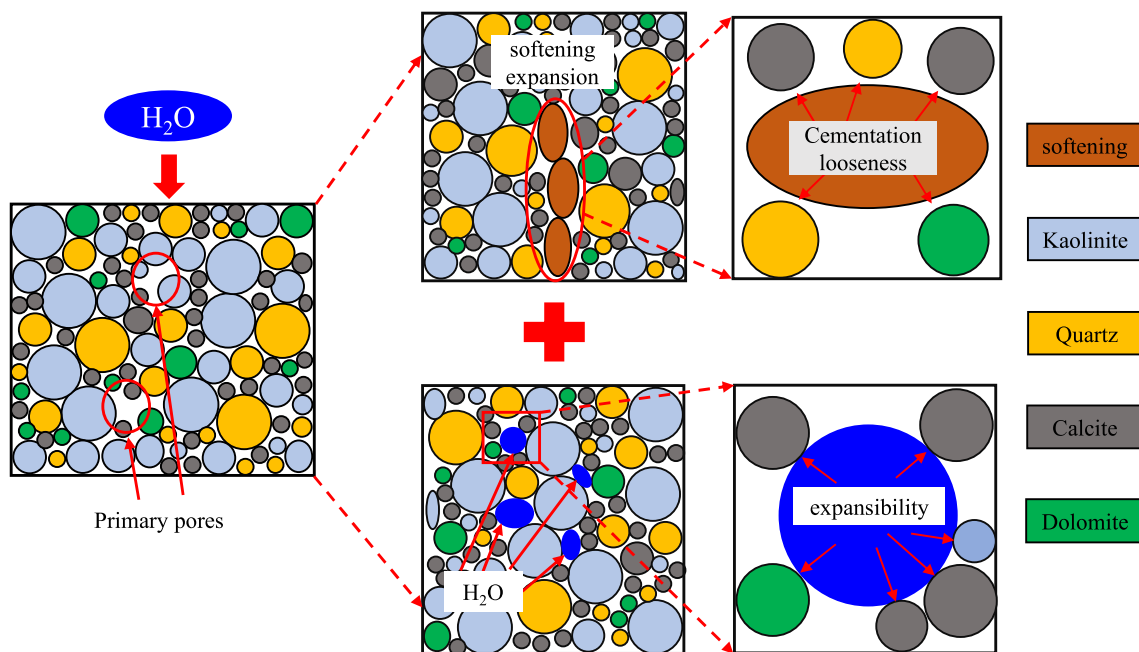**Fig. 24** Micro mechanism of water content on strength in Mohr's circle

Fig. 23 Mechanism diagram of coal seam water injection softening

5.2 Energy mechanism of water on coal burst prevention

According to Li et al. (2019), brittleness index can be defined as the comprehensive ability of consuming a small amount of energy in different stages, which has definitions of: (1) For pre-peak stage, most of energy is stored as ESE. (2) Rock failure depends more on the releasing of ESE. (3) At the post-peak stage, the ESE is completely dissipated. According to these definitions, brittleness index consists of three sub-parameters B_1, B_2, and B_3. The brittleness index B_1 is the first stage, which can be expressed as:

$$B_1 = \frac{U_p^e}{U_p} \tag{12}$$

At same time, a parameter W, which named additional energy, can be expressed as:

$$W = \int_{\varepsilon_{ap}}^{\varepsilon_{ar}} \sigma_a d\varepsilon_a = \frac{1}{2}(\sigma_p + \sigma_r)(\varepsilon_{ar} - \varepsilon_{ap}) \tag{13}$$

where ε_{ar} is the axial residual strain, ε_{ap} is the peak axial strain.

The ratio of released elastic strain energy ΔU^e to the driving energy reflects the self-maintenance failure ability of the rock, which can be expressed as:

$$\frac{\Delta U^e}{W + \Delta U^e} = \frac{U_p^e - U_r^e}{W + U_p^e - U_r^e} \tag{14}$$

According to the characteristics of post-peak stage of stress strain curve, failure modes can be divided into two types. (1) Rock failure requires additional energy ($W > 0$). In this case, the value of Eq. (11) is less than 1. (2) Rock failure does not require additional energy ($W \leq 0$), and the value of Eq. (11) is equal to 1. This unstable failure mode is usually considered as absolute brittle failure. Based on this classification, brittleness index B_2 can be defined as:

$$B_2 = \begin{cases} \frac{\Delta U^e}{W + \Delta U^e}, & W > 0 \\ W > 0, & W \leq 0 \end{cases} \tag{15}$$

The dissipation degree of cumulative ESE can be quantified by parameter B_3, which is calculated as follows:

$$B_3 = 1 - \frac{U_r^e}{U_p^e} \tag{16}$$

The total brittleness index B is then obtained by the following:

$$B = B_1 \cdot B_2 \cdot B_3 \tag{17}$$

Figure 25 shows that the relationship curves between brittleness indexes and water content. It can be seen that the brittleness index decreases linearly as the water content increase (Fig. 25a). Under uniaxial compression conditions, the average brittleness indexes are 0.65 (0%), 0.43 (0.6%), 0.41 (1.08%), 0.37 (1.5%), 0.27 (2%), and 0.18 (2.3%), respectively. Therefore, brittleness index of the coal sample gradually decreases when water content increase from 0% to 2.3%, which also means that the mechanical property gradually transforms from brittleness to plasticity.

Based on the definitions of sub brittleness indexes, as shown in Fig. 25b, c, and d. It is obvious that parameters B_1, B_2, and B_3 show negatively related to water content with different sensitivity. With the water content increased from 0% (dry state) to 2.3% (natural saturation state), the decrease rate ($\Delta B / \Delta w$) are 5.22, 21.3, and 9.13 for B_1, B_2, and B_3, respectively. Therefore, the sensitivity of parameter B_2 to water content is higher than parameter B_1 and B_3. Therefore, according to definitions shown in Eq. (15), water content in coal mainly influences the dissipation rate and dissipation degree of cumulative ESE in the post-peak stage.

Based on the brittleness index B, obtained the relationship curve between brittleness index and average particle size and IEI. As shown in Fig. 26, it can be clearly seen that with increase of brittleness index, the average fragment size shows a nonlinear increased trend (the blue line), while the IEI decreases nonlinearly (the red line). When the brittleness index increases from 0.18 to 0.41, the average particle size decreases from 38.38 to 30.89 mm. When the brittleness index continues to increase from 0.41 to 0.43, the average particle size decreases rapidly from 30.89 to 26.28 mm. When the brittleness index increases from 0.43 to 0.65, the average particle size changes little. This is consistent with the definition of brittleness index. As the brittleness index increases, the coal sample gradually transforms from plasticity to brittleness, so the particle size increased. Besides, when the brittleness index increases from 0.18 to 0.43, the IEI increases slowly from 1.71 to 4.02. With brittleness index increases to 0.65, the IEI increases to 4.85.

Therefore, as increases in water content, the brittleness index decreases and mechanical property of coal changes to ductility gradually. As a result, the failure mode transitions from typical brittle failure (splitting ejection) to ductile failure (shear), and average fragment size increases accompanied with change of failure mode. Besides, with decreasing of brittleness index B_2, the dissipated post-peak energy increased gradually, which finally results in decreasing of impact energy index and burst proneness.
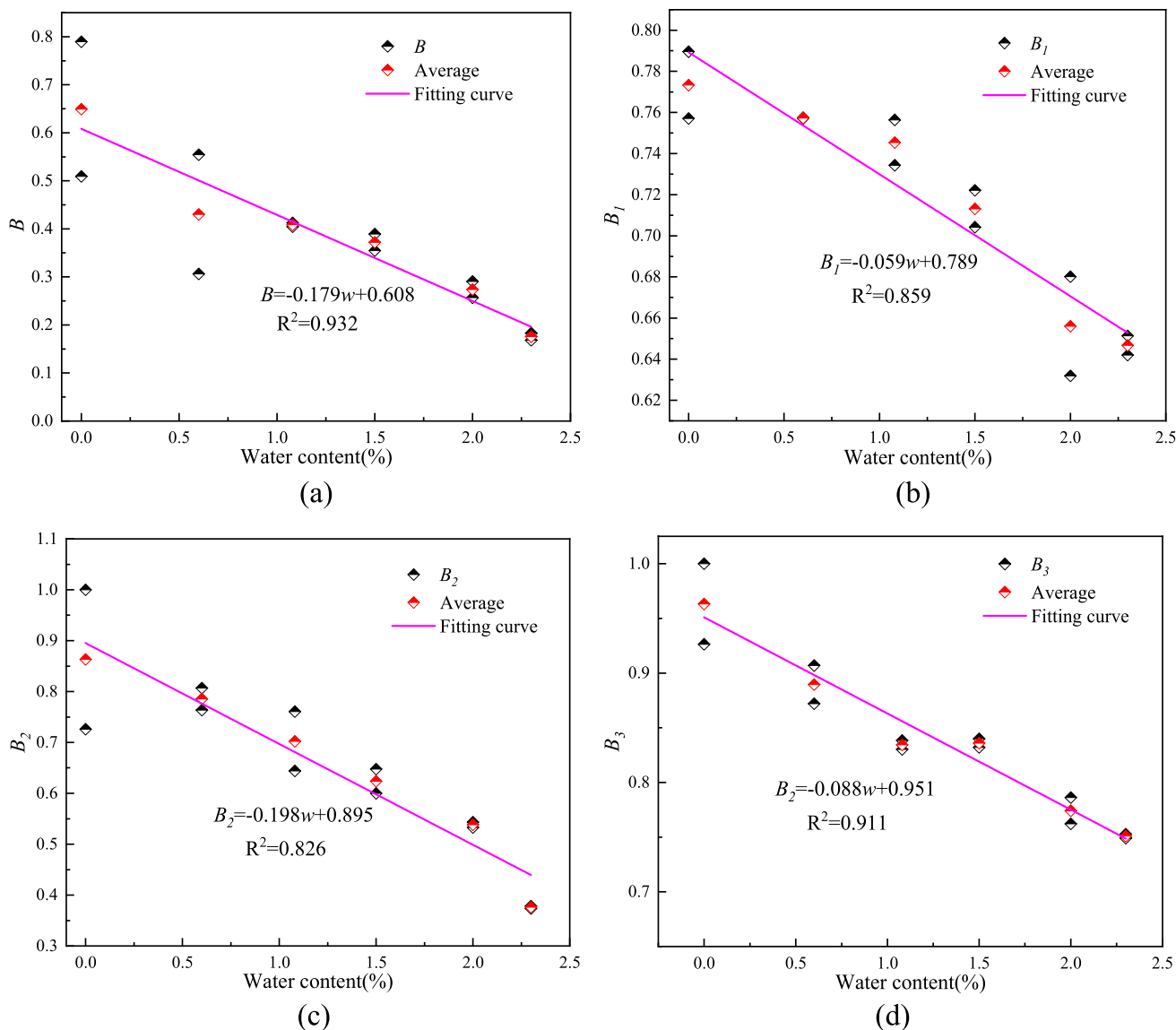
Fig. 25 Relationship between brittleness index and water content: **a** Brittleness index B; **b** Brittleness index B_1; **c** Brittleness index B_2; **d** Brittleness index B_3

5.3 Engineering significance

The coal burst, as a severe disaster in coal mining engineering, is easily induced by mining stress and impact load. The huge release of energy causes coal fragments injected from surface into roadways with a high velocity, which threat to the safety of coal mining seriously. Many ways to be used to prevent in underground.

When apply water injection to prevent coal burst in practice, many factors determine effectiveness of preventions measures, including geostress conditions, structures in coal seam, mechanical properties of coal, distribution of water injection holes, and water injection pressure (Konicek

et al. 2018). Generally, two effective means, changing water injection hole and increasing water pressure, can relieve coal burst as all known. Therefore, the influence of these two factors on coal burst was discussed by a series of numerical simulations in this study. During simulation, a parameter, namely saturation zone ratio (S_r), has been defined as the ratio of area of saturated to the whole area of coal seam to analyze effectiveness of prevention.

Two different water injection holes distributions, including three and five holes, have been considered here. From numerical simulation model in Fig. 15, three holes indicate only W1, W3, and W5 existed in the model. According to Fig. 27a, when injection pressure (P) increases from 0.5 to
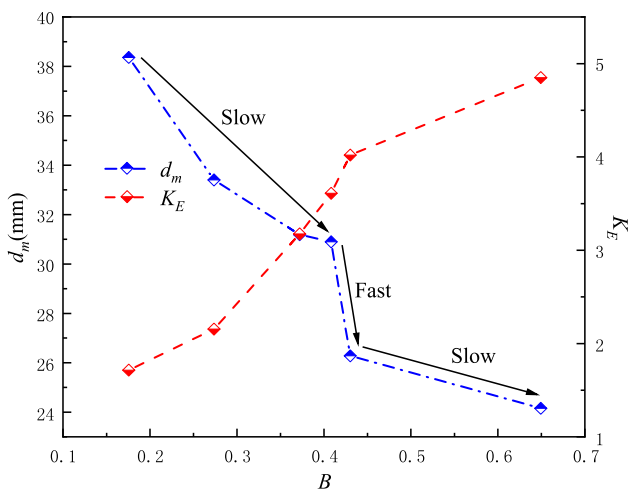
Fig. 26 The relationship between brittleness index and average fragment size and impact energy index

5 MPa, Sr for both of three holes and five holes keep increasing. Overall, for different holes distribution, the Sr increase rapidly when increasing injection pressure initially, and then the growth rate gradually slows down. As shown in Fig. 27a, there is an obvious transition zone with a pressure range of 2.0–3.0 MPa. That is, when injection pressure over 3 MPa, the increasing rate of Sr is small, which means increases injection pressure is hard to increase saturated zone area. Besides, five holes are easier to reach saturation than three holes. When injection pressure is 5 MPa, the coal seam for five holes condition almost reaches the maximum Sr, while the value of Sr for three holes is just equal to that of five holes with injection pressure of 2.8 MPa. Therefore, water injection pressure and holes distribution are equivalent to a certain extent.
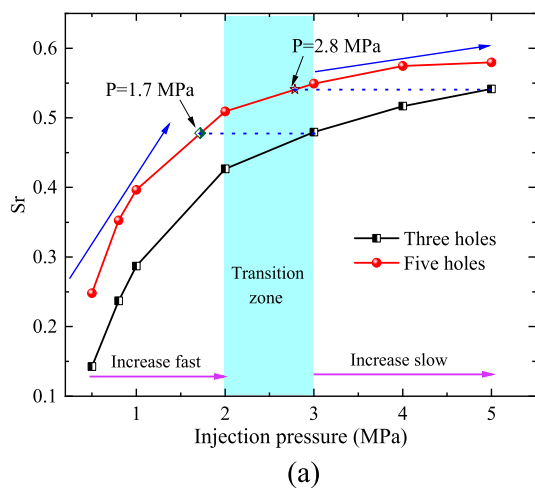
Moreover, Fig. 27b showed displacements and velocities of point B under different injection pressure with five injection holes. With increasing injection pressure, the displacement first decreases and then increases, while block velocity keeps decreasing. Compared characteristics of displacement and velocity, two stages can be divided in this process. At the first stage (water injection pressure is less than 2 MPa), the displacement and velocity decrease simultaneously. The main mechanism of water injection is softening, which reduces the coal burst proneness. At the second stage (the water injection pressure is more than 2 MPa), the block velocity almost keeps constant (decreased by 0.15 m/s), while the displacement increases rapidly. At this time, the coal burst proneness is in a stable state. The main reason for the increase of displacement is that the water pressure between the cracks of the coal seam reduces the effective stress, making an easier failure of coal. At this point, increasing water pressure has already been a negative factor for coal mining safety.

Therefore, even increasing water injection pressure can increase saturation and reduce number of water injection holes, it may also increase displacement and cause the failure. In summary, after the distribution of water injection holes is fixed, a critical water injection pressure is needed to search out in practice. Future study is necessary to develop a critical criterion according to influence factors listed above.

6 Conclusions

To investigate effect of water on failure and energy characteristics of coal and mechanism of coal burst prevention by water injection, a series of uniaxial compression in combination of SEM tests were carried out on coal specimens
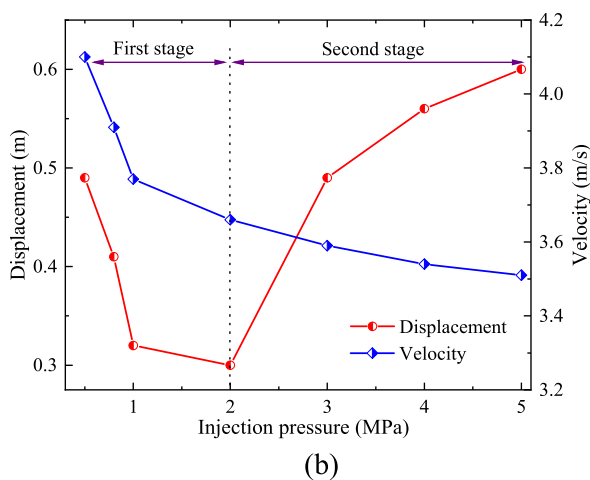
Fig. 27 Influence factors on coal burst: **a** Water injection holes distribution; **b** Injection pressure

with five different water contents, and a numerical model containing roadway excavation was established considering the water on coal burst prevention. The following conclusions can be drawn:

(1) The uniaxial compression tests results indicated that UCS, total energy, elastic strain energy, dissipated energy, as well as impact energy index decrease as water content increases. However, with increasing water content, the elastic strain energy ratio decreases, while the dissipated energy ratio increases. Therefore, the water in coal causes increase in proportion of dissipated energy, which finally results in decreasing of impact energy index and burst proneness.

(2) With increasing water content, the coal samples transition gradually from splitting ejection to tensile-shear mixed failure mode, while the average fragment size of failure samples increases gradually. Besides, as increases in water content, the brittleness index decreases and mechanical property of coal changes to ductility gradually, which are the main reason for changing of failure mode and fragment size.

(3) The SEM tests results indicated that softening effect of water on coal includes two aspects. Firstly, the soften and expansion of minerals increases the numbers of internal pores. As a result, the internal cohesion and friction angle between adjacent mineral particles decreased. Besides, water existed in pores between minerals particles reduced the effective stress. The combination of above two parts finally causes the decrease of coal macroscopical strength.

(4) Numerical results revealed that the increased water content can reduce degree of coal burst and ejection velocity of coal blocks, while it will raise up the depth of crack zone and surface displacement of roadway. Besides, water injection pressure and holes distribution are equivalent to a certain extent, and increase in water injection pressure may result in increased displacement and cause an easier failure. Therefore, the distribution of water injection holes and critical water injection pressure should be balanced in practice.

Author contributions LXW—Conceptualization, Validation, Data Curation, Writing-Review& Editing; CHX—Conceptualization, Methodology, Software, Data Curation, Writing; LB—Validation, Writing-Review& Editing; WS—Conceptualization, Software, Data Curation, Writing; LQS—Supervision; LY—Review & Editing; LJ—Review & Editing.

Declarations

Conflict of interest The authors have no conflict of interest to declare that are relevant to the content of this article.

References

Bai QS, Zhang C, Young RP (2022) Using true-triaxial stress path to simulate excavation-induced rock damage: a case study. Int J Coal Sci Technol 9:49

Chang JC, He K, Pang DD, Li D, Li CM, Sun BJ (2021) Influence of anchorage length and pretension on the working resistance of rock bolt based on its tensile characteristics. Int J Coal Sci Technol 8(6):1384–1399

Dou L, Yang K, Chi X (2020) Fracture behavior and acoustic emission characteristics of sandstone samples with inclined pre-cracks. Int J Coal Sci Technol 8(1):77–87

Du C, Bi J, Zhao Y, Wang C (2022) A stratified NMR-based investigation of spatial evolution of pore structure in sandstone after cyclic heating and local water cooling. Nat Resour Res 31(6):3365–3392

Gu H, Tao M, Cao W, Zhou J, Li X (2019) Dynamic fracture behaviour and evolution mechanism of soft coal with different porosities and water contents. Theoret Appl Fract Mech 103:102265

Han J, Wu C, Wang Z, Zhang S, Wang Z (2023) Experimental study of water distribution affected by stress sensitivity and pore–fracture compressibility of low-rank coals with different levels of water saturation. Nat Resour Res 1–23

Hao D, Tu S, Zhang C (2020) Experimental study on the effect of moisture content on bituminous coal porosity based on 3D reconstruction of computerized tomography. Nat Resour Res 29:1657–1673

He M, Ren F, Liu D (2018) Rockburst mechanism research and its control. Int J Min Sci Technol 28(5):829–837

Jiang L, Xu Y, Chen B, Wu B (2021) Effect of water content on the mechanical properties of an artificial porous rock. Bull Eng Geol Env 80(10):7669–7681

Konicek P, Waclawik P (2018) Stress changes and seismicity monitoring of hard coal longwall mining in high rockburst risk areas. Tunn Undergr Space Technol 81:237–251

Li N, Zou Y, Zhang S, Ma X, Zhu X, Li S, Cao T (2019) Rock brittleness evaluation based on energy dissipation under triaxial compression. J Petrol Sci Eng 183:106349

Li CC, Zhao T, Zhang Y, Wan W (2022) A study on the energy sources and the role of the surrounding rock mass in strain burst. Int J Rock Mech Min Sci 154:105114

Li N, Jin ZJ, Wang HB, Zou YS, Zhang SC, Li FX, Zhou T, Jiang MQ (2023) Investigation into shale softening induced by water/CO_2-rock interaction. Int J Rock Mech Min Sci 161:105299

Liu Z, Cao A, Guo X, Li J (2018) Deep-hole water injection technology of strong impact tendency coal seam-a case study in Tangkou coal mine. Arab J Geosci 11:1–9

Liu XW, Chen HX, Liu QS, Liu B, He J (2022a) Modelling slurry flowing and analyzing grouting efficiency under hydro-mechanical coupling using numerical manifold method. Eng Anal Bound Elem 134:66–78

Liu XW, Chen HX, Liu B, Deng W, Liu QS, Zhang Z (2022b) Experimental and numerical study on failure characteristics and mechanism of coal under different quasi-static loading rates. Theor Appl Fract Mech 121:103478

Ma D, Duan HD, Zhang JX, Bai HB (2022) A state-of-the-art review on rock seepage mechanism of water inrush disaster in coalmines. Int J Coal Sci Technol 9:50

Mi C, Zuo J, Sun Y, Zhao S (2022) Investigation on rockburst mechanism due to inclined coal seam combined mining and its control by reducing stress concentration. Nat Resour Res 31(6):3341–3364

Pan C, Xia B, Zuo Y, Yu B, Ou C (2022) Mechanism and control technology of strong ground pressure behaviour induced by high-position hard roofs in extra-thick coal seam mining. Int J Min Sci Technol 32(3):499–511

Shen J, Shu Z, Cai M, Du S (2020) A shear strength model for anisotropic blocky rock masses with persistent joints. Int J Rock Mech Min Sci 134:104430

Si L, Wei J, Xi Y, Wang H, Wen Z, Li B, Zhang H (2021) The influence of long-time water intrusion on the mineral and pore structure of coal. Fuel 290:119848

Vishal V, Ranjith PG, Singh TN (2015) An experimental investigation on behaviour of coal under fluid saturation, using acoustic emission. J Nat Gas Sci Eng 22:428–436

Weng L, Wu Z, Liu Q, Wang Z (2019) Energy dissipation and dynamic fragmentation of dry and water-saturated siltstones under sub-zero temperatures. Eng Fract Mech 220:106659

Wei C, Zhang C, Canbulat I, Huang W (2021) Numerical investigation into impacts of major fault on coal burst in longwall mining-a case study. Int J Rock Mech Min Sci 147:104907

Wang T, Yan CZ (2023) Investigating the influence of water on swelling deformation and mechanical behavior of mudstone considering water softening effect. Eng Geol 318:107102

Yao Q, Chen T, Tang C, Sedighi M, Wang S, Huang Q (2019) Influence of moisture on crack propagation in coal and its failure modes. Eng Geol 258:105156

Zhang S, Li Y, Shen B, Sun X, Gao L (2019) Effective evaluation of pressure relief drilling for reducing rock bursts and its application in underground coal mines. Int J Rock Mech Min Sci 114:7–16

Zhang SK, Lu L, Wang ZM, Wang SD (2020) A physical model study of surrounding rock failure near a fault under the influence of footwall coal mining. Int J Coal Sci Technol 8(4):626–640

Zhang X, Tang J, Pan Y, Yu H (2022) Experimental study on intensity and energy evolution of deep coal and gas outburst. Fuel 324:124484

Zhang C, Bai QS, Han PH, Lei W, Wang XJ, Wang FT (2023) Strength weakening and its micromechanism in water-rock interaction, a short review in laboratory tests. Int J Coal Sci Technol 1(10):10

Zhou Y, Wu Z, Weng L, Liu Q (2021) Seepage characteristics of chemical grout flow in porous sandstone with a fracture under different temperature conditions: an NMR based experimental investigation. Int J Rock Mech Min Sci 142:104764